Producing a magnetically anisotropic soft material: synthesis of iron oxide nanoparticles in a carrageenan/PVA matrix and stretching of the hybrid gelatinous bulk

AUTHOR(S):

Sakai, Rie; Teramoto, Yoshikuni; Nishio, Yoshiyuki

CITATION:

Sakai, Rie ...[et al]. Producing a magnetically anisotropic soft material: synthesis of iron oxide nanoparticles in a carrageenan/PVA matrix and stretching of the hybrid gelatinous bulk. Polymer Journal 2018, 50(3): 251-260

ISSUE DATE:

2018-03

URL:

http://hdl.handle.net/2433/254359

Producing a magnetically anisotropic soft material: Synthesis of iron oxide nanoparticles in a carrageenan/PVA matrix and stretching of the hybrid gelatinous bulk

Rie Sakai[a], Yoshikuni Teramoto[b, c*], and Yoshiyuki Nishio[a]

[a] Division of Forest and Biomaterials Science, Graduate School of Agriculture, Kyoto University, Kyoto 606-8502, Japan
[b] Department of Applied Life Science, Faculty of Applied Biological Sciences, Gifu University, Gifu 501-1193, Japan
[c] Center for Highly Advanced Integration of Nano and Life Sciences (G-CHAIN), Gifu University, Gifu 501-1193, Japan

(Dr. Y. Teramoto, Department of Applied Life Science, Faculty of Applied Biological Sciences, Gifu University, Gifu 501-1193, Japan)
E-mail: teramoto@gifu-u.ac.jp

Running head: Magnetically anisotropic carrageenan/PVA/Fe_3O_4

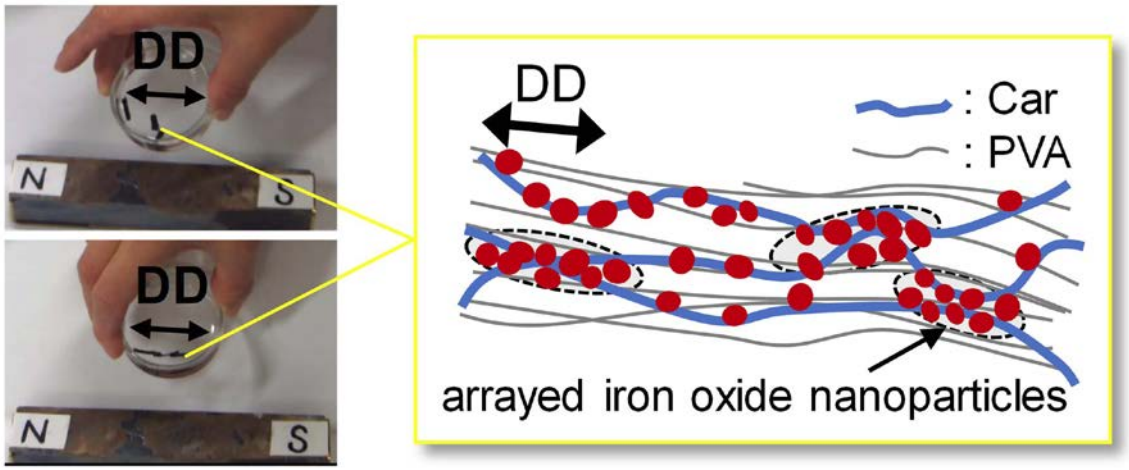

We propose a method for preparing magnetic anisotropic soft materials. That includes a chemical loading (*in-situ* synthesis) of iron oxide nanoparticles in a matrix composed of κ-carrageenan (Car) and poly(vinyl alcohol) (PVA), followed by mechanical stretching of the hybrid in a wet process. Anionic Car was used for accommodating iron oxide nanoparticles and it was blended in advance with PVA having an ability of high orientation. Scanning electron microscopy revealed that the loaded granular iron oxide nanoparticles (50–100 nm) formed elliptical clusters by drawing the hybrid composite. Wide angle X-ray diffraction indicated that the PVA constituent was oriented in the draw direction. With the orientation of the composite matrix, the iron oxide nanoparticles formed therein would gather to develop the elliptical clusters. The drawn samples showed different amplitudes in the magnetization ($M_{\parallel} > M_{\perp}$) when measured in two setups where the applied field was parallel (||) or perpendicular (⊥) to the draw direction. Specific responses of the drawn sheets to an external magnetic stimulus were visualized, and they were reasonably attributed to an effect of the magneto-anisotropy coming from the preferred orientation of the nanoparticle aggregates.

carrageenan/poly(vinyl alcohol)/magnetic anisotropy

INTRODUCTION

Magnetic nanocomposites of eco-friendly or biocompatible polysaccharides[1–21] have potentials for various applications. They include filtration and separation green systems, information transfer and storage media, fabrics for electromagnetic wave shielding, field-sensitive actuators and sensors, magnetic drug-delivery systems and other biomedical products, etc.

We have reported a series of studies in which iron ions were chelated to anionic polysaccharides and then they were oxidized *in situ* via $Fe(OH)_2$ production to form iron oxide nanoparticles.[9,12,17,21] We have established conditions of regulating the amount and size of magnetic iron oxide nanoparticles; thereby it has been possible to obtain hybrids containing superparamagnetic (SPM) iron oxide particles of several tens of nanometers. For instance, by repeating the *in-situ* synthesis cycle 3–4 times within a carrageenan (Car) matrix, magnetic composites that gave a high saturation magnetization (M_s) reaching ~25 emu/g-sample at 298 K were easily obtained without impairing the SPM character.[17]

In a recent work using a combination of cellulose nanocrystal (CNC)/Car as matrix, we reported that the iron oxide-containing nanocomposites exhibited a “shape magneto-

anisotropy" after appropriate treatment to array the magnetic nanoparticles.[21] The concept of material design was based on the following idea: the magnetic iron oxide nanoparticles were synthesized *in situ* in the CNC/Car matrix; the nanocomposites obtained in sheet form were subjected to a drawing process to invite orientation; thereby the distance between the magnetic nanoparticles which were originally finely dispersed became close enough to allow the magnetic walls to move, even though there were solely separate magnetic domains before the orientation treatment. The resulting spheroidal clusters behaved virtually as ferromagnets, although the original magnetic nanoparticles themselves were isotropic granular ones and imparted SPM.[21] Eventually, a demagnetizing field was induced inside the nanocomposite samples in different amplitudes varying with the external magnetic vector, and a macroscopic anisotropic magnetization was accomplished.

In the present study, we propose a method to prepare nanocomposites with magnetic anisotropy more simply. For this purpose, Car (κ-type) was blended with poly(vinyl alcohol) (PVA) and used as a matrix. Both the component polymers are supplied as general industrial raw materials. The microcomposition can be done in a simple process of mixing Car and PVA aqueous solutions. For this combination, compatibility has been evaluated from the melting point depression data of the PVA component.[22] Recently, an attempt has been made to prepare Car/PVA composites as an adsorbent for cationic dye; magnetite nanoparticles were incorporated into the composites in order to easily recover the absorbent with a magnet.[23] On the other hand, we here expect that the Car having sulfo groups is a necessary component for intercalating iron ions to produce magnetic iron oxide while the other PVA constituent stretches the entire matrix to provide an anisotropically aggregated array structure of iron oxide particles. With PVA, its microcrystals and hydrogen bonding interaction behave like crosslinking points, so it is assumed that high deformation of the entire matrix including amorphous regions is possible. For PVA gel alone, it was impossible to effectively incorporate iron oxide by this *in-situ* method.[9] Basically, meanwhile, it is difficult to largely deform the matrix of κ-type of Car which gives elastic gels.[24,25] The combination of Car and PVA is thus useful.

In order to demonstrate this concept, we first examined the compatibility of Car and PVA by differential scanning calorimetry (DSC) from the glass transition behavior. After that, magnetic iron oxide was *in-situ* synthesized in the composite matrix in a similar manner of our previous studies. We tried to optimize the process of stretching gel-like nanocomposites containing iron oxide nanoparticles. The nanocomposites were then subjected to wide-angle X-ray diffraction and morphological observation to

characterize the orientation behavior of the composites and the distribution state of the iron oxide nanoparticles. The magnetic anisotropy was evaluated with a superconducting quantum interference device (SQUID). We will also exemplify several patterns of anisotropic response of the products to external magnetic stimuli.

EXPERIMENTAL PROCEDURES

Original materials

The carbohydrate polymer sample of Car was a commercial product of κ-carrageenan (Copenhagen Pectin Ltd., GENUGEL WR-78-J, lot no. 035400), and the molecular weight and the sulfur content (S) have been determined in the preceding study;[17] M_w = 8.28 ×10^5, M_w/M_n = 2.21, and S = 5.97 wt%. PVA was supplied as PVA-HC by Kuraray Co.; the nominal degree of polymerization was 1750 and the saponification value was 99.9 mol%.

Ferrous chloride tetrahydrate ($FeCl_2 \cdot 4H_2O$) and H_2O_2 aqueous solutions were obtained from Wako Pure Chemical Ind., Ltd., and all the other chemicals and solvents used were guaranteed reagent grade and employed without further purification. However, water (usually distilled one) and ethanol involved in the synthesis of iron oxides in polymer composite gels were degassed with N_2-bubbling in advance of the use.

Iron oxide incorporation into Car/PVA gels

Aqueous solutions of Car and PVA were prepared separately at concentrations of 5.0 and 10 wt%, respectively; the original polymer materials were dissolved in water at 95 ºC with continuous stirring. The solutions were mixed in the hot state so that the solid weight ratio of Car/PVA was 20/80 and the mixture was stirred for 30 min at that temperature. The Car/PVA weight ratio (20/80) was adopted in consideration of stretchability of the composite (see later discussion). The hot mixture was poured into a rectangular Teflon tray and transformed into a hydrogel by cooling naturally to room temperature (23 ºC).

The Car/PVA gel was then immersed in an excess amount of ethanol/water mixture (23 ºC) containing $FeCl_2$ at a concentration of 0.10 M. The ethanol/water mixture used in this study was prepared by mixing at a volume ratio of 1:1. After the immersion in the salt solution for 2 h, the Fe^{2+}-intercalated gel was lightly washed with ethanol/water and steeped in 1.0 M NaOH solution in ethanol/water (pH ≈ 13) for 2 h to produce ferrous hydroxide in the polymer composite network. The system whole (300 mL flask) was heated to 65 ºC, and 2.0-wt% H_2O_2 solution in ethanol/water was added dropwise into the alkaline medium over a period of 15 min. The oxidized gel (dark reddish brown color)

was taken out from the container and washed with ethanol/water. Gel samples thus once oxidized were further oxidized in two cycles involving the ferrous ion-intercalation, alkali treatment, and oxidization with hydrogen peroxide. The sequence of procedures for the *in-situ* synthesis of iron oxide in the gel matrix was basically similar to that applied to PVA-free carrageenan gels in the preceding study.[17] A portion of the respective gel products (Car/PVA/Fe) was cut away and stored in a refrigeration until the use for magnetometry measurements, and the rest was provided for a step for preparing drawn sheets.

Preparation of drawn sheets of Car/PVA/Fe

An iron oxide-containing gel sample with a moisture content of ~90 wt% was diced into small pieces and placed in a 50-mL beaker. The beaker was placed in a water bath at 65 ºC and the sample in the beaker was stirred with a glass rod to make it into a sol state. The sol sample was put into a micropipette and then discharged from the pipette into *t*-butyl alcohol (*t*-BuOH) (30 ºC) stirred at 800 rpm. The stirring was continued for 10 min. Thereafter, the resulting fibrous cylindrical samples were taken out from *t*-BuOH, and the samples were each stretched to ~4 times its original length in a wet state using tweezers in the air at 23 ºC. The samples after the stretching had a diameter of 1.8 mm and were cut to 12 mm in length. The stretched sample was fixed on a glass slide with an adhesive tape, air-dried and vacuum-dried, and then subjected to subsequent measurements. Even though the sample in the wet state was in the form of a fibrous cylindrical shape, the sample after drying became a smooth surface sheet; the size was 12 mm in length, 2 mm in width, and 0.45 mm in thickness. Similarly, the sheet samples of as-spun state were prepared. The diameter immediately after extrusion with a micropipette was about 5 mm, and after drying with the ends fixed it became a sheet with a width of 5.5 mm and a thickness of about 1 mm.

Measurements

Differential scanning calorimetry (DSC) was conducted for Car/PVA composites with different weight ratios with a Hitachi High-Tech Science Corporation DSC6200/EXSTAR6000 apparatus. The measurements were performed on 7-mg samples under a nitrogen atmosphere after calibrating the temperature readings with an indium standard. The samples were first heated to 250 °C and immediately quenched to −140 °C. Then the second scans were run from −140 °C to 260 °C to record stable thermograms. The glass transition temperature (T_g) was determined from the midpoint of the discontinuity in heat flow.

The content of iron in the Car/PVA/Fe composite was measured by a redox titration method similar to that previously reported.[17]

Magnetometry measurements were carried out on air-dried sheet samples of 2-mm wide and 5-mm long with a superconducting quantum interference device (SQUID), MPMS-5 of Quantum Design Inc. The magnetic field (H) applied was varied through the cycle of 0 T → 5 T → −0.1 T → 0 T at a constant temperature. For a given sample, the magnetization (M) vs H data were collected at 298 and 100 K. With regard to drawn sheets, the draw direction (DD, major axis of specimens in this case) was set parallel (∥) or perpendicular (⊥) to the applied field; thereby two definable magnetizations, $M_{\parallel}$ and $M_{\perp}$, were estimated. The temperature dependence of magnetization (M vs T) was also examined in the so-called zero-field-cooled (ZFC) and field-cooled (FC) conditions. The field strength applied was 0.01 T, and the experimental procedure has been described in the previous papers.[17, 21, 26]

Morphological observations were made using a field emission scanning electron microscope (FE-SEM), Hitachi S-4800. The samples were sputter-coated with Pt before the observation.

Wide-angle X-ray diffraction (WAXD) measurements were made using a Rigaku diffractometer R-AXIS RAPID II. The apparatus was operated at 50 kV and 100 mA, and Ni-filtered CuKα radiation (0.154 nm) was utilized.

Evaluation of the macroscopic responsive behavior to an external magnetic field

For visual observation of the magnetic field response, larger specimens were prepared. For this purpose, the Car/PVA sol sample containing iron oxide at 65 ºC was poured into a Teflon container (20 mm width × 40 mm length × 10 mm depth, each inside dimension), and 30-ºC *t*-BuOH was gradually added into the vessel to form a gel. The gel sample was allowed to stand for 10 min in the *t*-BuOH bath, stretched three times of its original length using a hand-cranked drawing device in the air at 23 ºC, and air-dried while being attached to the drawing device to prepare a sheet specimen. The obtained samples were appropriately cut out and used. Gels that were solely air-dried without being stretched were used as as-cast samples for reference. In addition, the gels which were stretched but cut without drying were subjected to observation as water-swollen Car/PVA/Fe specimens.

Several test pieces cut from the drawn sheets were provided for observation of the macroscopic responsive behavior to an external magnetic field. The observation was performed by the following two ways: (1) The test pieces were floated on ethanol in a Petri dish, and a bar magnet of 0.15 T was employed for the field application. (2) A

rectangular water-swollen Car/PVA/Fe sample was cut out so that the bottom was almost square and two different color tapes were affixed to the opposing side-faces, respectively. A thread was attached to one end of the sample and it was suspended where the DD was perpendicular to the gravitational field. A 0.15-T bar magnet was brought close to the sample and its movement was observed.

RESULTS AND DISCUSSION

In the present study, anionic Car was responsible for incorporating iron oxide nanoparticles and it was combined with PVA showing an ability of high orientation. We thereby attempted to control the distribution state of the magnetic iron oxide nanoparticles by stretching the nanocomposites whole, to demonstrate magnetically anisotropic materials.

In order to evaluate the compatibility of Car and PVA and determine an appropriate proportion, different compositions of Car/PVA were subjected to DSC measurements to detect a possible variation of glass transition temperature (T_g) with the changing composition. The composites were prepared by solution casting from mixtures of the respective aqueous solutions. The DSC thermograms obtained in the second heating scan are shown in Figure 1. As can be seen in Figure 1a, the T_gs of Car alone and Car-rich composites were unclear, but the T_g of PVA component rose as the Car content increased. Based on such a systematic T_g shift, we judged that there was a good compatibility between the components in the amorphous regions of the composite series. For the PVA-rich compositions (Car/PVA = 30/70 to 0/100), the melting point of PVA appeared at 200 ºC or higher, as shown in Figure 1b. The melting point depression and broadening were conspicuous as Car content increased, and the crystal domain of PVA disappeared in Car-rich blends. This is similar to general behavior of amorphous/crystalline polymer pairs showing good compatibility. On the other hand, we found a gap as to the T_g shift between 20 and 30 wt% in the Car content. When the Car content is lowered to 20 wt% or less, it appears that the physical properties such as thermal transition of the composites are similar to those of PVA. In the present study, therefore, the Car/PVA proportion was fixed to 20/80 by weight, in anticipation of high orientation of the nanocomposites and as much iron oxide loading as possible. The validity of selecting this composition will be demonstrated by the stretching behavior described below.

As a result of the redox titration, the iron content was determined to be 9.2 wt% for the Car/PVA/Fe nanocomposite prepared by repeating the *in-situ* synthesis of iron oxide three times. Because Car has sulfate groups, it was possible to prepare the composite in

which iron ions were easily incorporated into the matrix and iron oxide particles were accommodated in large amounts.

In the drawing process, an aqueous sol-like sample (Car/PVA = 20/80 in weight) containing iron oxide was extruded by a micropipette into a gel form in a *t*-BuOH bath, and after a while it was taken out and stretched in the air. The time to immerse the gel in *t*-BuOH was the best for 10 min. When it was stretched with tweezers, it could be extended to four times the original length. Preliminary experiments showed that the compositions containing more than 20% Car could not deform more than 1.5 times; the κ-type of Car basically gives a highly elastic gel.[24,25] Incidentally, other coagulation baths (methanol, ethanol, and 2-propanol) were also tried, but *t*-BuOH was the most suitable in respect of stretchability of the wet nanocomposites. This may be attributable to the speed of coagulation; the coagulation rate of the present sample decreased in the order of methanol, ethanol, 2-propanol, and *t*-BuOH uses. The slower coagulation and precipitation in *t*-BuOH would also be advantageous for the gel sample to hold the flexibility and deformability of the constituting polymer network for a longer time. Thus the Car/PVA/Fe nanocomposites could easily be stretched.

The samples subjected to the following various characterizations were as-spun samples (via micropipette extrusion) and those stretched with tweezers; each was air-dried with both ends fixed on a glass slide, to form a nearly rectangular sheet. For comparison, we also show several data of as-cast sheets obtained by air-drying the sol.

FE-SEM images of the surfaces of as-cast, as-spun, and drawn samples are shown in Figure 2. For the as-cast sample, it was observed that granular particles considered as iron oxide were randomly dotted as shown in Figure 2a. On the other hand, Figure 2b indicates that iron oxide particles were distributed on the surface of the as-spun sample. The size of the particles estimated from the image was 50–100 nm, and these particles seemed to partially aggregate and be slightly aligned along the extrusion direction (ED). With regard to the surface of the sample stretched four times (Figure 2c), it was confirmed that the iron oxide particles were gathered and arranged along the drawing direction (DD) to form array structures (typically, <1 μm length and <200 nm diameter). The diameter of the individual iron oxide particles was 50–100 nm as in the case of the as-spun specimen. For the drawn sample, a bundle-like morphology (< 1 μm width) was also developed, seemingly appearing in fibrous orientation at a low magnification.

Figure 3 illustrates WAXD data for sheets of Car/PVA/Fe. DD and ED of the samples were set to be perpendicular to the equator of the WAXD diagram, as exemplified for the sheet drawn four times in Figure 3a. The diagram was characterized by composition of diffractions from two kinds of crystals, spinel ferrite of Fe_3O_4 and PVA,

as indexed for a few intense diffractions on the photograph. As shown in Figure 3b, slight preferential orientation was observed in the diffraction of (311) plane of the iron oxide unit in the four-time stretched sample, although the peak was broad. However, it was hardly observed in the as-spun samples. With regard to PVA crystal (Figure 3c), the azimuthal scanning of the (101) diffraction at $2\theta = 19.5^\circ$ showed no significant change in intensity for the as-cast sheet. The azimuthal profiles of the as-spun and drawn sheets, meanwhile, exhibited maxima on the equator (azimuthal angle $\phi = 0$ and 180°). It was thus found that the PVA crystals in the as-spun sample preferentially oriented along the ED by extruding from the micropipette and regeneration in the coagulation bath. When the sample was stretched, the peaks in the azimuthal scan became somewhat sharper. This suggests an improvement of crystallinity and orientation in the drawing and drying processes, although it is necessary to further investigate into the formation and growth of PVA crystals. Also, there is a possibility that the orientation of amorphous chains was improved as well.

SQUID magnetometry was conducted for the samples and an effect of the structural anisotropy was evaluated. For the measurements, we used smaller specimens cut out from the oriented sheets into a rectangular form of 5 mm in the ED or DD direction and 2 mm in the one perpendicular thereto. As-cast sheets cut into 2-mm square were provided for the measurements, too.

Figure 4 shows magnetization (M) versus applied field (H) plots at 298 K for the air-dried specimens. As can be seen in the enlarged ones ((a)'–(c)'), any of the samples imparted a perceptible hysteresis in the range of −0.05–0.05 T, by which the magnetism at this temperature was judged to be ferromagnetic (FM), although the extent of the hysteresis loop was generally small or moderate. We have reported so far that similar FM behavior was observed at 100 K for some parallel composites prepared by three-time repetition of the *in-situ* synthesis of iron oxide in the matrices containing Car.[17,21] To give FM means that the size of each iron oxide particle is reasonably large. That magnetism was consistent with the observation of iron oxide particles with 50–100 nm diameter by FE-SEM.

Figure 5 illustrates ZFC and FC curves obtained for the three samples in an applied field of 0.01 T. As can be seen in Figure 5a, no clear maximum was observed in the ZFC curve for the as-cast sample. The FC and ZFC curves were close to each other at room temperature (300 K), but they were separated at slight lower temperature and the divergence became remarkable with decreasing temperature. The fact that the temperature at which FC and ZFC curves separated was close to room temperature was consistent with the tendency of the composite to show FM at room temperature. The

tendency was basically the same, regardless of processing routes and *M*-measuring directions, as can be seen from the data in Figure 5b and c.

As for the influence of orientation, the magnetization ($M_{\parallel}$) of the as-spun and drawn sheets in the parallel set was always larger than that ($M_{\perp}$) in the perpendicular set. The result indicates that the axis of easy magnetization lies parallel to ED or DD of the sheets, respectively. The magnetic anisotropy, represented by a ratio $M_{\parallel}/M_{\perp}$, was generally higher in the drawn sample and particularly at lower field strengths, when compared at a constant temperature of 298 K (see Table 1). In Figure 5b and c, the ZFC and FC data for the two samples, each shown in both parallel and perpendicular sets, demonstrate the anisotropy of magnetization at 0.01 T over a wide range of temperature; plainly, the drawn sample is superior to the as-spun sample in the degree of the anisotropy.

Concerning the magnetic anisotropy observed above, probably the macroscopic shape anisotropy of the samples themselves was partly contributive to the observation, because the specimens were cut out so that the principal (longer) axis was in the DD or ED direction. Nevertheless, it should be noted that the drawn and as-spun specimens were shaped into a similar rectangular form for the SQUID measurements. Here, we consider the microscopic scale, that is, the state of individual magnetic nanoparticles. Because we observed no substantial shape anisotropy and no explicit crystallite orientation for the iron oxide (Fe_3O_4) nanoparticles by FE-SEM and WAXD, respectively, each magnetic nanoparticle (virtually round-shaped) can be taken to hardly show magnetic anisotropy. In interpretation of the above observation, we thus assume that the distance between the magnetic nanoparticles was close enough to allow the domain wall to move and they formed a cluster following deformation of the polymer matrix. This would have been significant in the drawn specimen that showed a particularly high anisotropy of magnetization. Actually, the FE-SEM data (Figure 2c) indicated that the loaded iron oxide particles in the drawn sheet assembled to make an array along DD. As modeled in Figure 6, the individual aggregates can be regarded as an oriented magnetic body of prolate ellipsoid. When this body is subjected to an external field H_{ex}, a so-called demagnetizing field H_d is induced inside in the direction opposite to H_{ex}; the intensity of H_d is stronger along the shorter axis than along the longer axis of the ellipsoid.[27] This results in the incidence of anisotropy ($M_{\parallel} > M_{\perp}$) as to the magnetization which is expressed as $M = \chi(H_{ex} - H_d)$ with susceptibility χ.

The formation of such oriented elliptical magnetic bodies was more clearly supported by visual observation of the responsiveness of the drawn (three times) sample as a whole to an external magnetic field. Figure 7 illustrates results of the observation for test pieces of rectangular shape cut from a drawn sheet. The longer axes of the strips were

perpendicular (Figure 7a) or parallel (Figure 7b) to DD, respectively. They were floated on ethanol in a Petri dish. When the Petri dish was brought close to a bar magnet (0.15 T), the strips rotated so that the DD and the force lines of the magnet were parallel to each other regardless of the cutting directions.

As a control experiment, the magnetic field response was similarly evaluated for as-cast samples as well. When the in-plane aspect ratio was ~1, the as-cast samples were not rotated but just attracted to the magnet. In the use of rectangular shapes, however, the cast samples uniformly moved so that the longer axes were invariably parallel to the magnetic flux lines.

The different manners in magnetic response observed above for the nanocomposite sheets are interpretable in terms of an effect of shape anisotropy.[27] However, the dimension scale of the anisotropy and therefore the structural factor was largely different between the drawn sheet and the as-cast one. In the drawn sheets, the loaded iron oxide nanoparticles were assembled in a larger aggregate (typically, <1 μm length and <200 nm diameter) to make an array along DD. As modeled in Figure 6, the individual aggregates can be regarded as an oriented magnetic body of prolate ellipsoid. On the other hand, the as-cast sheet had no preferred arrangement of granular iron oxide nanoparticles. In this situation, only the macroscopic shape itself can be a source of magnetic anisotropy. Therefore, when the as-cast sheet was cut into rectangular strips, their respective longer axes became the easy axis of magnetization. For the strips of the drawn sheet, however, it is reasonable to take that the shape anisotropy in micro-texture, rather than that in the outward of sample, more greatly contributed to the anisotropy of material magnetization. This was manifested by the magnetic orientation behavior (Figure 7a) of the strips whose longer axis was cut perpendicularly to DD.

Another magnetic response experiment enabled us to confirm the microscopic magnetic anisotropy of our oriented samples as well. As shown in the middle of Figure 8, we suspended a water-swollen Car/PVA/Fe specimen in which the basal plane was substantially square and the DD was perpendicular to the plane of the paper. When a bar magnet was put close to it, the specimen rotated and the DD and magnetic force became parallel. If the N and S poles of the magnet were exchanged, the specimen rotated in the opposite direction. Because the bottom of the samples was almost square and there was no influence of anisotropy due to the shape of the whole sample, the effect of microscopic magnetic anisotropy of the drawn sample has been more clearly confirmed. If the sample DD was in the vertical direction, namely, perpendicular to the force lines of the magnet, the sample was just attracted to the magnet without rotating.

In extension of these results, we can make a diversity of orientation patterns of strips

in a static magnetic field, if the strips are cut at various angles to DD from the drawn nanocomposites. From a more practical standpoint, the drawn nanocomposites explored here serve as an example of functional materials that can provide magneto-responsive microchips of <100 μm sizes, each having a prescribed axis of orientation; the chips would be applicable to a micro-patterning element controlled by magnetic force.

CONCLUSION

Magnetic iron oxide nanoparticles were *in-situ* synthesized in a compatible Car/PVA polymer matrix. By stretching the obtained magnetic nanocomposite in a gel state, the iron oxide nanoparticles loaded inside virtually formed elliptical magnetic clusters. As a result, we succeeded in making the composites anisotropically responsive to an external magnetic field. Here Car and PVA were responsible for carrying over iron and orientation, respectively, into the nanocomposites. These constituents are industrially familiar raw materials, and the preparation process for the nanocomposites is simple. Although the magnetic iron oxide nanoparticles accommodated in the composites were granular and did not show a remarkable anisotropic magnetization by themselves, the microscopic rearrangement was accomplished successfully to develop a macroscopic magnetization anisotropy. We believe that this method can be applied as a practical one for easily obtaining magnetically anisotropic materials.

ACKNOWLEDGEMENTS

The authors acknowledge Dr. A. Otsuka of the Research Center for Low Temperature and Materials Science, Kyoto University, for his technical support in the SQUID magnetometry measurements. This work was partially financed by a Grant-in-Aid for Scientific Research (A) (No. 26252025 to Y.N.) from the Japan Society for the Promotion of Science.

1. Marchessault, R. H., Ricard, S. & Rioux, P. *In situ* synthesis of ferrites in lignocellulosics. *Carbohydr. Res.* **224,** 133–139 (1992).
2. Raymond, L., Revol, J. F., Marchessault, R. H. & Ryan, D. H. *In situ* synthesis of ferrites in ionic and neutral cellulose gels. *Polymer* **36,** 5035–5043 (1995).
3. Kroll, E., Winnik, F. M. & Ziolo, R. F. *In situ* preparation of nanocrystalline γ-Fe_2O_3 in iron(II) cross-linked alginate gels. *Chem. Mater.* **8,** 1594–1596 (1996).
4. Sourty, E., Ryan, D. H. & Marchessault, R. H. Characterization of magnetic membranes based on bacterial and man-made cellulose. *Cellulose* **5,** 5–17 (1998).

5. Veiga, V., Ryan, D. H., Sourty, E., Llanes, F. & Marchessault, R. H. Formation and characterization of superparamagnetic cross-linked high amylose starch. *Carbohydr. Polym.* **42,** 353–357 (2000).
6. Jones, F., Cölfen, H. & Antonietti, M. Interaction of kappa-carrageenan with nickel, cobalt, and iron hydroxides. *Biomacromolecules* **1,** 556–563 (2000).
7. Suber, L., Foglia, S., Ingo, G. M. & Boukos, N. Synthesis, and structural and morphological characterization of iron oxide-ion-exchange resin and -cellulose nanocomposites. *Appl. Organomet. Chem.* **15,** 414–420 (2001).
8. Chatterjee, J., Haik, Y. & Chen, C. J. Biodegradable magnetic gel: Synthesis and characterization. *Colloid Polym. Sci.* **281,** 892–896 (2003).
9. Nishio, Y., Yamada, A., Ezaki, K., Miyashita, Y., Furukawa, H. & Horie, K. Preparation and magnetometric characterization of iron oxide-containing alginate/poly(vinyl alcohol) networks. *Polymer (Guildf).* **45,** 7129–7136 (2004).
10. Si, S., Kotal, A., Mandal, T. K., Giri, S., Nakamura, H. & Kohara, T. Size-controlled synthesis of magnetite nanoparticles in the presence of polyelectrolytes. *Chem. Mater.* **16,** 3489–3496 (2004).
11. Daniel-da-Silva, A. L., Trindade, T., Goodfellow, B. J., Costa, B. F. O., Correia, R. N. & Gil, A. M. In situ synthesis of magnetite nanoparticles in carrageenan gels. *Biomacromolecules* **8,** 2350–2357 (2007).
12. Matsumoto, Y., Teramoto, Y. & Nishio, Y. Preparation of thermoplastic magnetic wood via etherification and *in-situ* synthesis of iron oxide. *J. Wood Chem. Technol.* **30,** 373–381 (2010).
13. Olsson, R. T., Azizi Samir, M. a S., Salazar-Alvarez, G., Belova, L., Ström, V., Berglund, L. a, Ikkala, O., Nogués, J. & Gedde, U. W. Making flexible magnetic aerogels and stiff magnetic nanopaper using cellulose nanofibrils as templates. *Nat. Nanotechnol.* **5,** 584–8 (2010).
14. Li, G., Du, Y., Tao, Y., Deng, H., Luo, X. & Yang, J. Iron(II) cross-linked chitin-based gel beads: Preparation, magnetic property and adsorption of methyl orange. *Carbohydr. Polym.* **82,** 706–713 (2010).
15. Liu, S., Zhou, J. & Zhang, L. In situ synthesis of plate-like Fe_2O_3 nanoparticles in porous cellulose films with obvious magnetic anisotropy. *Cellulose* **18,** 663–673 (2011).
16. Katepetch, C. & Rujiravanit, R. Synthesis of magnetic nanoparticle into bacterial cellulose matrix by ammonia gas-enhancing in situ co-precipitation method. *Carbohydr. Polym.* **86,** 162–170 (2011).
17. Oya, K., Tsuru, T., Teramoto, Y. & Nishio, Y. Nanoincorporation of iron oxides into

carrageenan gels and magnetometric and morphological characterizations of the composite products. *Polym. J.* **45,** 824–833 (2013).

18. Zhou, J., Li, R., Liu, S., Li, Q., Zhang, L., Zhang, L. & Guan, J. Structure and magnetic properties of regenerated cellulose/Fe_3O_4 nanocomposite films. *J. Appl. Polym. Sci.* **111,** 2477–2484 (2009).
19. Nypelö, T., Rodriguez-Abreu, C., Rivas, J., Dickey, M. D. & Rojas, O. J. Magneto-responsive hybrid materials based on cellulose nanocrystals. *Cellulose* **21,** 2557–2566 (2014).
20. Nypelö, T., Rodriguez-Abreu, C., Kolena'ko, Y. V., Rivas, J. & Rojas, O. J. Microbeads and hollow microcapsules obtained by self-assembly of Pickering magneto-responsive cellulose nanocrystals. *ACS Appl. Mater. Interfaces* **6,** 16851–16858 (2014).
21. Yoshitake, H., Sugimura, K., Teramoto, Y. & Nishio, Y. Magnetic property of oriented films of cellulose nanocrystal/carrageenan composites containing iron oxide nanoparticles : Effect of anisotropic aggregation of the nanoparticles. *Polymer* **99,** 147–156 (2016).
22. Tanaka, T., Lu, T., Yuasa, S. & Yamaura, K. Structure and properties of poly(vinyl alcohol)/κ-carrageenan blends. *Polym. Int.* **50,** 1103–1108 (2001).
23. Mahdavinia, G. R., Massoudi, A., Baghban, A. & Shokri, E. Study of adsorption of cationic dye on magnetic kappa-carrageenan/PVA nanocomposite hydrogels. *J. Environ. Chem. Eng.* **2,** 1578–1587 (2014).
24. Nishinari, K. Longitudinal vibrations of high-elastic gels as a method for determining viscoelastic constants. *Jpn. J. Appl. Phys.* **15,** 1263–1270 (1976).
25. Hossain, K. S., Nemoto, N. & Nishinari, K. Dynamic viscoelasticity of iota carrageenan gelling system near sol-gel transition. *Nihon Reoroji Gakkaishi (Journal Soc. Rheol. Japan)* **25,** 135–142 (1997).
26. Gittleman, J. I., Abeles, B. & Bozowski, S. Superparamagnetism and relaxation effects in granular Ni-SiO_2 and Ni-Al_2O_3 films. *Phys. Rev. B* **9,** 3891–3897 (1974).
27. Cullity, B. D. & Graham, C. D. *Introduction to Magnetic Materials, 2nd Edition*. (John Wiley & Sons, 2011).

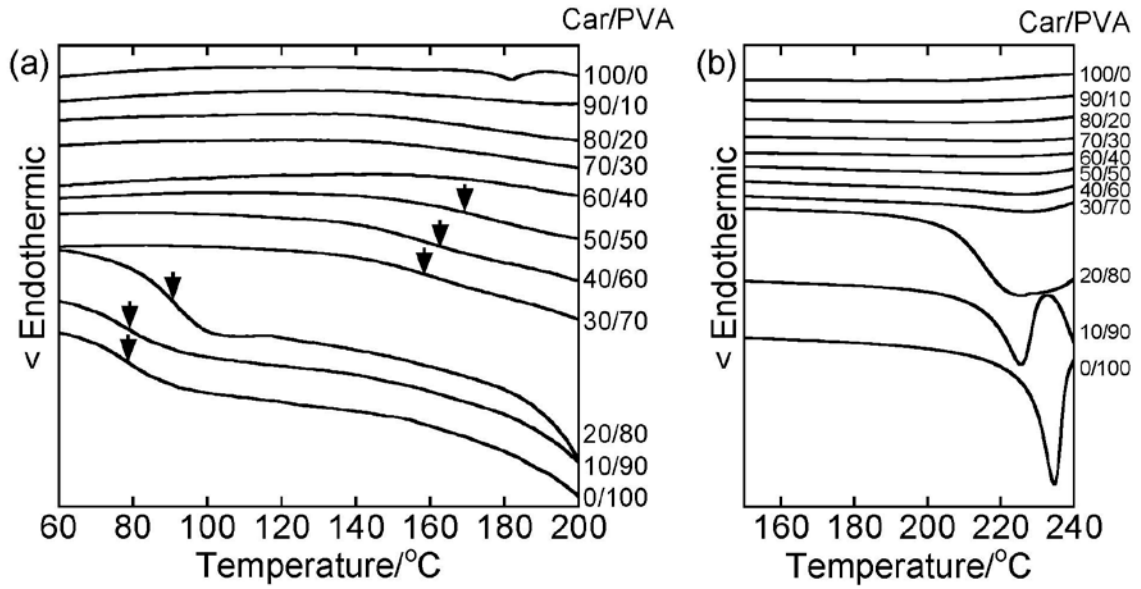

Figure 1 DSC thermograms of Car/PVA composites in the second heating scan. Mid-point T_g positions are indicated by arrows for the respective compositions in (a). Part (b) represents enlarged thermograms around the melting point of PVA.

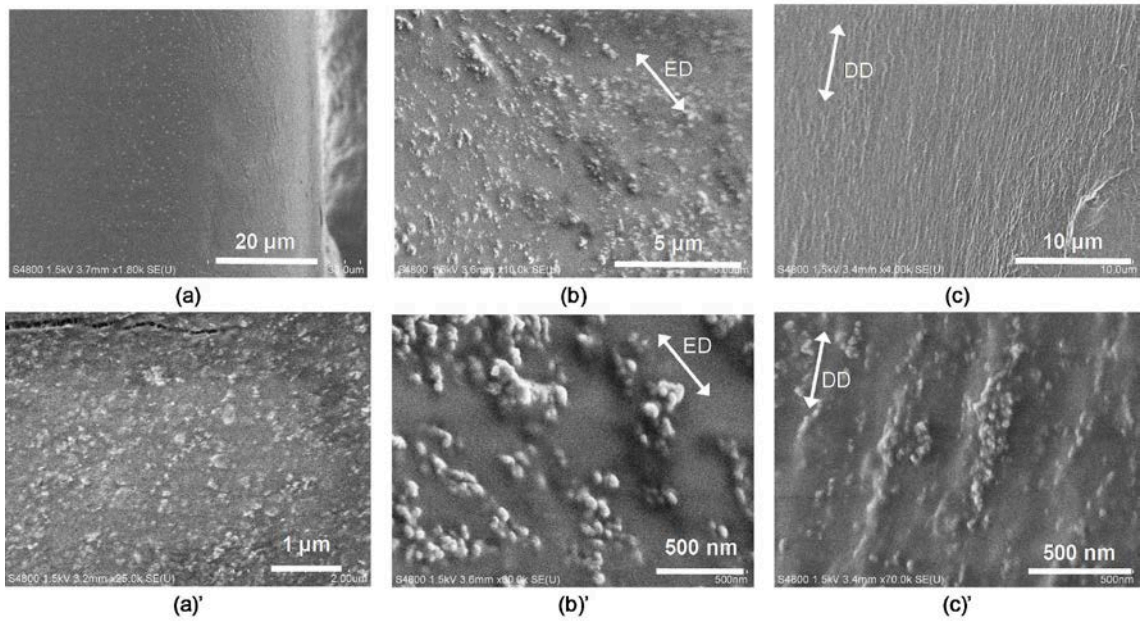

Figure 2 FE-SEM images for the surfaces of (a) as-cast, (b) as-spun, and (c) drawn (four times) sheets of Car/PVA/Fe. The image with the prime symbol shows each enlarged view.

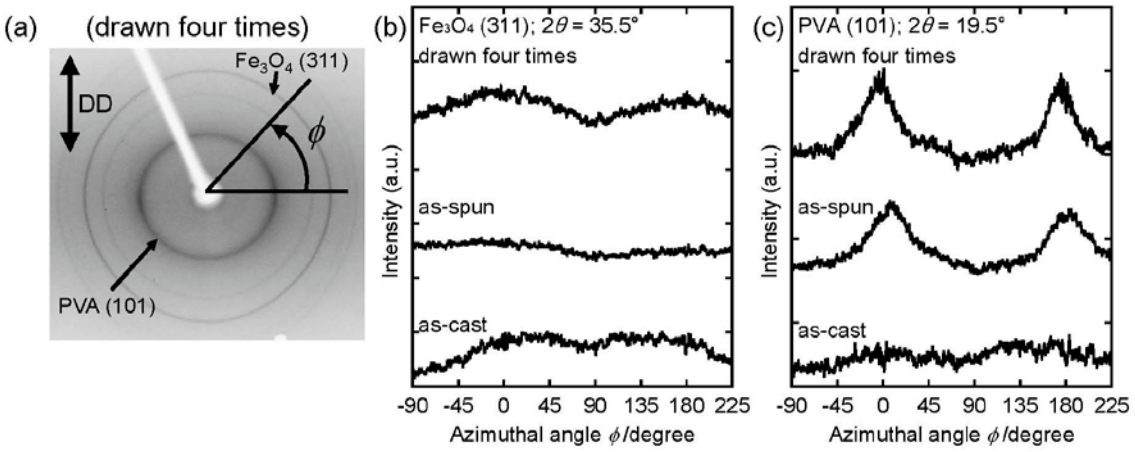

Figure 3 WAXD results for sheets of Car/PVA/Fe: (a) WAXD pattern of the sheet drawn four times, and azimuthal intensity profiles of (b) Fe_3O_4 (311) and (c) PVA (101) diffractions for as-cast, as-spun, and drawn (four times) sheets.

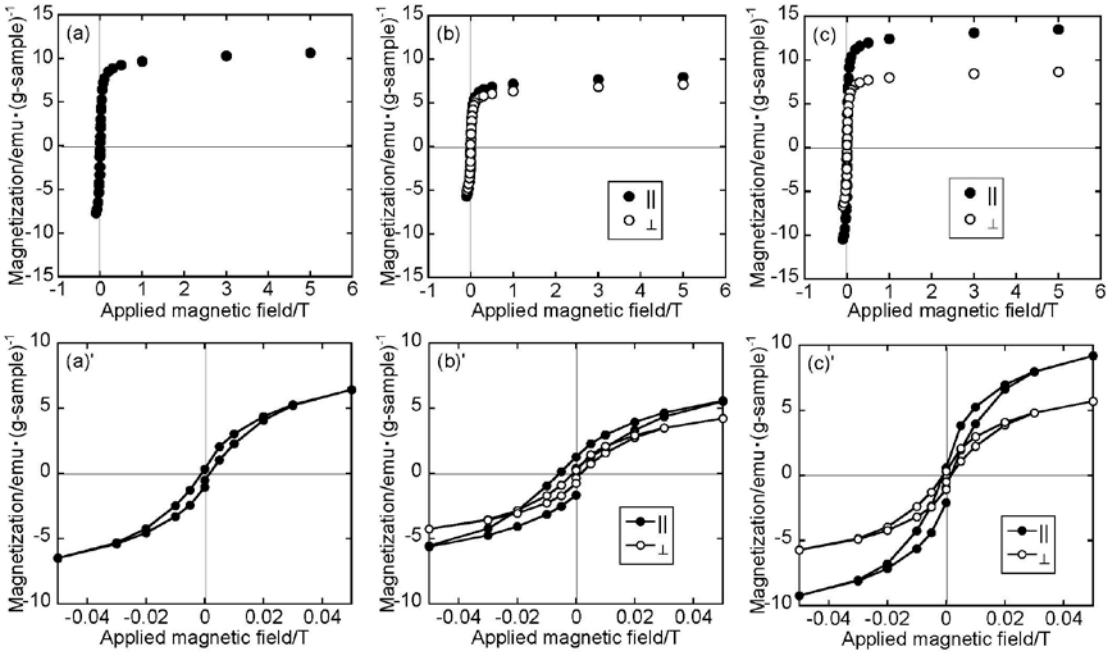

Figure 4 Magnetization vs. applied field plots at 298 K for (a) as-cast, (b) as-spun, and (c) drawn (four times) Car/PVA/Fe samples. The ones with the prime symbol added to (a)–(c) provide the data on an enlarged scale. Panels b and c include the magnetization data in two sets of ED and DD, respectively, parallel (∥) and perpendicular (⊥) to the applied field.

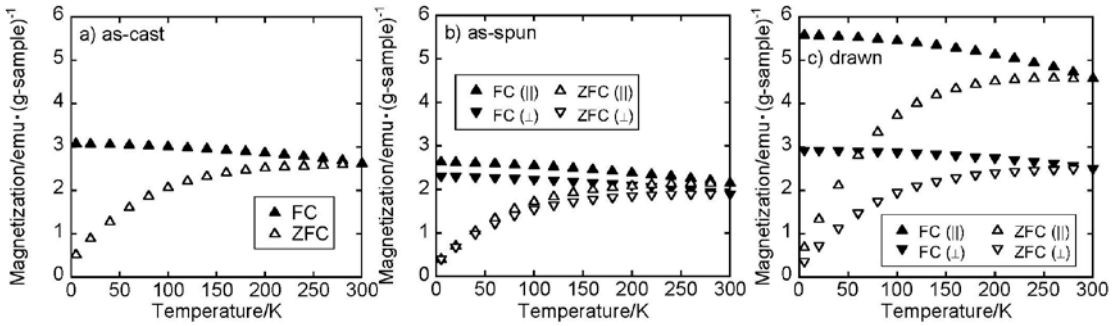

Figure 5 Temperature dependence of magnetization for (a) as-cast, (b) as-spun, and (c) drawn (four times) samples, examined with a field strength of 0.01 T in ZFC (open symbol) and FC (solid symbol) conditions. Panels b and c include the magnetization data in two sets of ED or DD, parallel (||) and perpendicular (⊥) to the applied field.

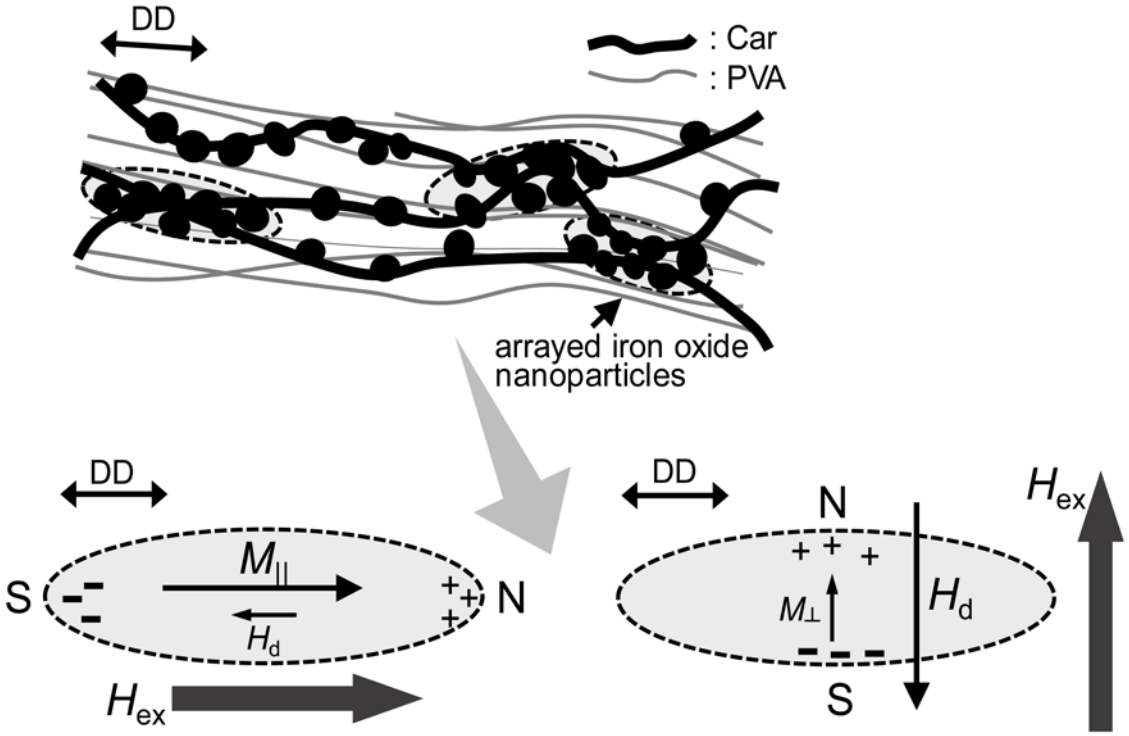

Figure 6 Pictorial representation that models the oriented aggregates of iron oxide nanoparticles distributed in a drawn matrix composed of Car and PVA and the magneto-anisotropy derived from the anisotropic micro-texture. The concept of this figure was reported in Fig. 9 of our previous paper.[21] (Rearranged with permission from Ref. 21: Copyright 2016 Elsevier Ltd.)

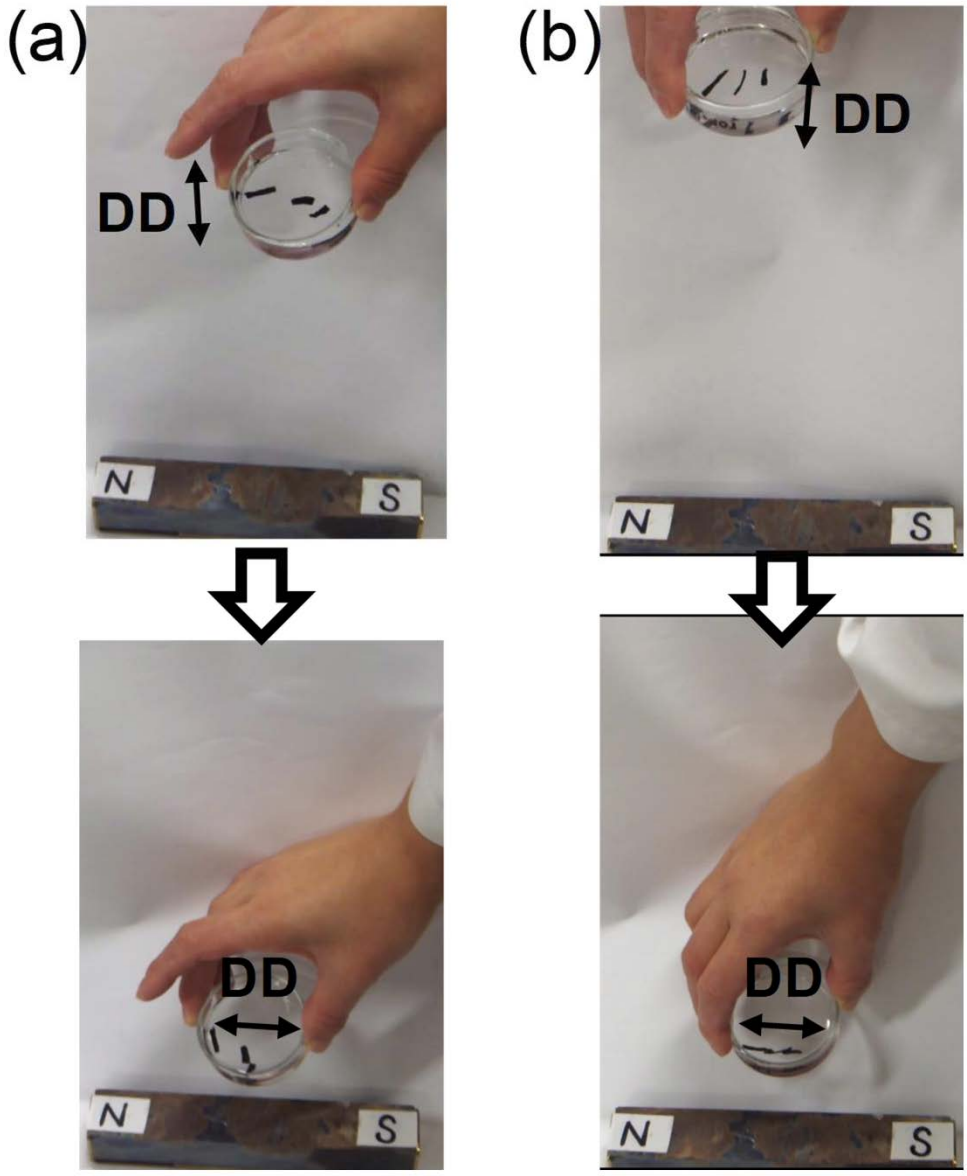

Figure 7 Photographic data showing magnetic orientation behavior of Car/PVA/Fe rectangular strips cut from a drawn sheet (draw ratio, three times): DD was (a) perpendicular and (b) parallel to the longer axis of the strips. The strips were floated on ethanol in a glass dish.

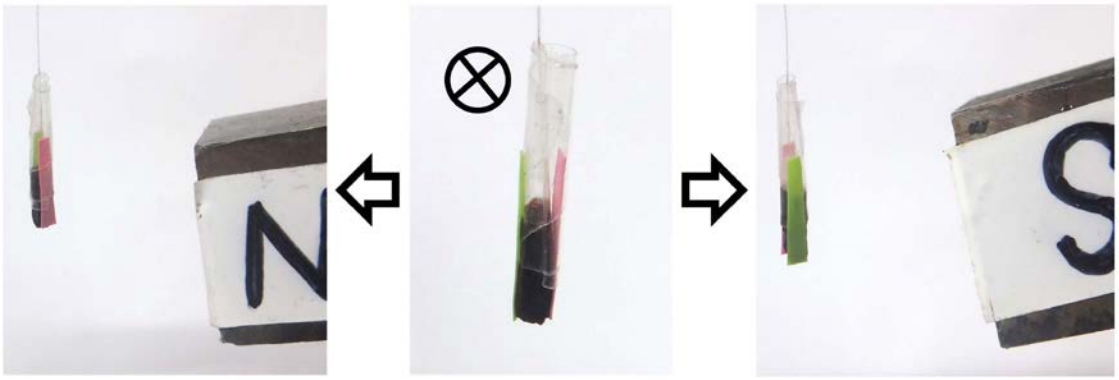

Figure 8 Response of a Car/PVA/Fe drawn sample swollen with water to a bar magnet. The gel sample was suspended in the vertical direction. The bottom surface of the sample was essentially square. As shown in the middle figure, the sample was first placed so that the DD was perpendicular to this page.

Table 1 $M_{\parallel}/M_{\perp}$ at different magnetic fields obtained by SQUID magnetometry at 298 K

	$M_{\parallel}/M_{\perp}$		
	at 0.005 T	at 0.050 T	at 3 T
as-spun	1.15	1.13	1.12
drawn	1.82	1.61	1.55